Unveiling Cognitive Processes Underlying Depression-like Behaviors in the Force Swim and Tail Suspension Tests

Zhihan Li, Tianyu Lu, Jiaozhao Yan, Xiang Zhang & Yun-Feng Li**

[1]Beijing Institute of Basic Medical Sciences, Beijing, China

[2]School of Life Science and Technology, ShanghaiTech University, Shanghai, China

[3]Beijing Institute of Pharmacology and Toxicology, Beijing Key Laboratory of Neuropsychopharmacology, Beijing, China

Keywords: forced swim tests, tail suspension tests, depression-like behaviors, cognitive processes, computational modeling, reinforcement learning models

Abstract

The forced swim test (FST) and tail suspension test (TST) are widely used to assess depression-like behaviors in rodents, with immobility time serving as a primary metric. However, this measure oversimplifies the complex cognitive processes involved, obscuring the relationship between immobility and cognitive biases. Here, we employ a custom-developed tool to capture complete behavioral trajectories in mice and apply reinforcement learning models for systematic analysis. Our findings indicate that behaviors in both tests can be interpreted as reinforcement learning processes that encompass learning, consequence perceiving, and decision-making. Notably, the underlying cognitive processes differ between the two tests, challenging the assumption that the FST and TST are interchangeable for cross-validation. Additionally, we exam two methods for inducing depression-like behavior: chronic restraint stress and medial prefrontal cortex inhibition. Both approaches increase immobility by altering learning dynamics and consequence sensitivity. Regression analyses further reveal two distinct behavior phases: an early phase dominated by learning-related factors and a later phase influenced by consequence sensitivity. These results suggests that conventional metrics focus solely on the final minutes of testing may underestimate learning processes while overemphasize sensitivity to consequences. Our study underscores the importance of computational modeling in revealing the complex cognitive mechanisms underlying animal behavior.

1. Introduction

Recent advances in rodent research have significantly advanced our understanding of the neural circuits and molecular mechanisms underlying mental disorders, establishing itself as a cornerstone of neuroscience and pharmacology[1–5]. However, rodents' inability to verbally express subjective experiences or perform complex cognitive tasks limits their ability to fully capture the cognitive distortions and information-processing abnormalities seen in conditions like depression[6–8]. To overcome this limitation, simplified behavioral models, such as the forced swim test (FST) and tail suspension test (TST), have been widely adopted[9–13]. These methods, shown in **Figure 1A** and **B**, have seen a significant increase in usage over the past two decades and continue to be some of the most popular behavioral assays (Figure 1C, D). The primary measure in these tests is immobility duration, which is often interpreted as an indicator of depression-like behavior (Figure 1J, K). However, this narrow focus on immobility overlooks the cognitive mechanisms that underlie these actions, raising questions about the true nature of what these tests measure. One promising explanation, the behavioral adaptation hypothesis, suggests that the gradual increase in immobility is part of an adaptive learning process[9,14–19]. Despite its prominence, empirical evidence supporting this hypothesis remains sparse, highlighting the need for further investigation into the cognitive processes that drive behavior in these tests.

A key challenge in understanding these cognitive processes lies in the limited scope of current behavioral metrics. Most studies reduce complex behaviors, typically measured over 5-6 minutes, to a single measure—total immobility time in the final minutes of the test (Figure 1E-H). This simplification obscures the underlying behavioral patterns that could offer deeper insights into cognitive mechanisms. As illustrated in Figure 1L, animals with identical immobility times may exhibit vastly different behavioral patterns driven by distinct cognitive processes. Although some pioneering studies have analyzed high-resolution behavioral trajectoires[10], these approaches often rely on labor-intensive manual annotations, limiting their scalability and broader application. Consequently, there is a growing need for automated tools that can efficiently track and generate fine-grained behavioral data, facilitating progress in research.

In addition to improving data collection methods, another challenge is interpreting this data to uncover the cognitive mechanisms behind observed behaviors. Computational modeling has emerged as a versatile methodological framework for formalizing latent cognitive computations underlying behavioral patterns, with growing applications in clinical investigations of psychiatric disorders[20–25]. This approach enables quantitative decomposition of behavior sequences across multiple experimental paradigms, including probabilistic reversal learning

(PRL)[26–29], Iowa gambling task (IGT)[30], fear conditioning[31] and two-stage decision[32,33]. These studies have successfully identified cognitive differences between individuals, particularly in how they process rewards and punishments[34–39]. For example, studies show that patients with depression exhibit altered reward sensitivity[25], prediction errors[40–42], and learning rates[43,44] compared to healthy individuals. Such findings have refined cognitive models of depression and provided a framework for better understanding mental disorders and developing effective treatments. Currently, there is a growing trend in animal studies to apply computational methods, such as reinforcement learning models, to analyze rodent behavior[45–49]. However, previous studies have focused primarily on operant learning tasks, while FST and TST, the most commonly used tests in studies of depression and anxiety, remain underexplored. The cognitive mechanisms driving depressive-like behaviors in these tests, as well as the cognitive biases associated with these behaviors, remain poorly understood.

This paper explores the cognitive processes underlying mice behavior in the FST and TST using reinforcement learning models, with the broader goal of developing new methods to exam implicit cognitive mechanisms in rodent research. We collected behavioral trajectories of mice using a custom-built tool, then applied several reinforcement learning models to interpret these behaviors. Our analysis demonstrates that the behavior observed in the FST and TST can be explained by different reinforcement learning processes. Furthermore, our analysis of model parameters suggests that behaviors at different stages of the tests are influenced by distinct cognitive components. This finding implies that traditional analytical methods, which often exclude the early stages of the test, may introduce biases in assessing cognitive processes.

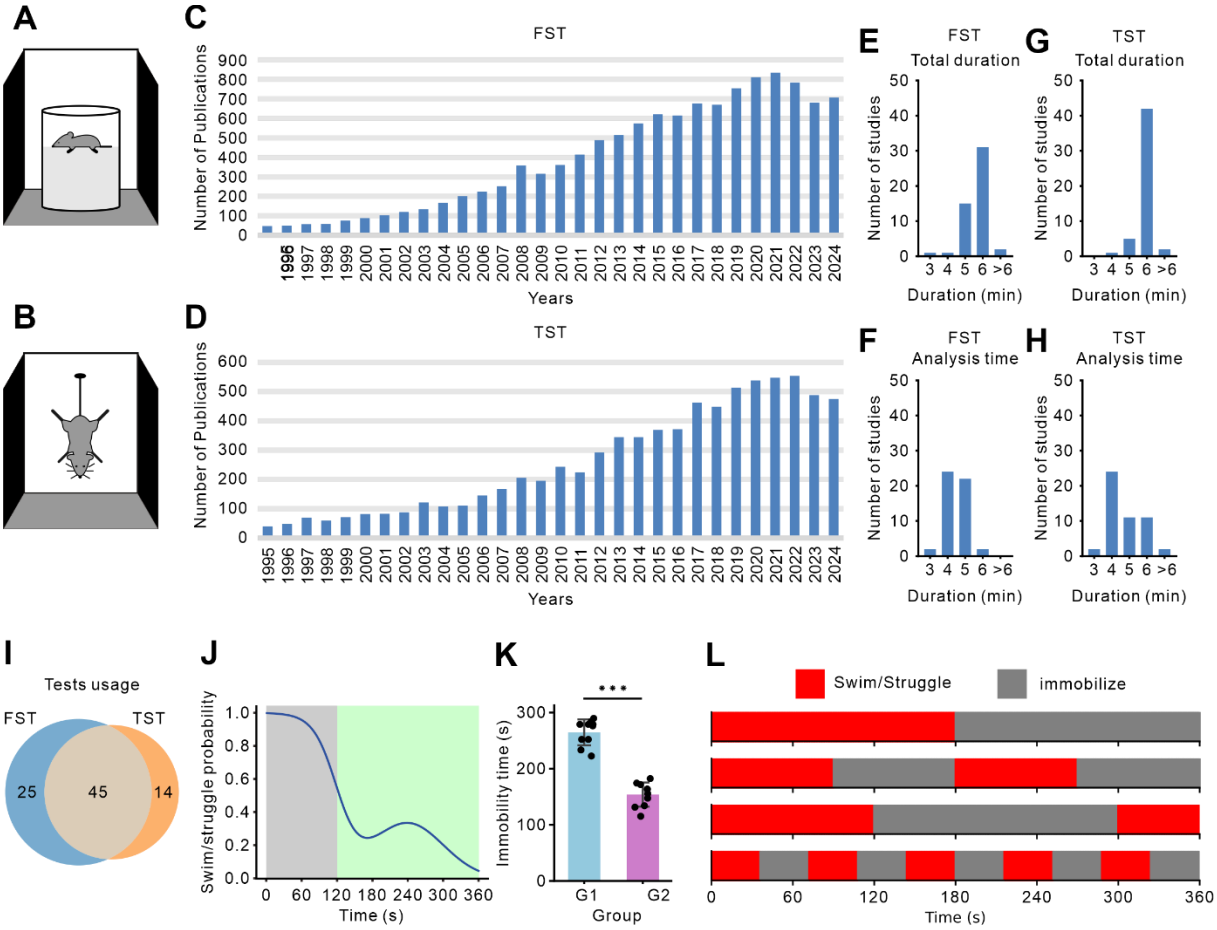

Figure 1. The forced swim test (FST) and tail suspension test (TST). A, B) Experimental setup for the FST and TST. In the FST (**A**), mice are placed in a container of water, while in the TST (**B**), they are suspended upside down. Both tests subject the mice to inescapable conditions for 5 to 6 minutes. In the FST, behaviors are classified as swimming or immobility, whereas in the TST, behaviors are categorized as struggling or immobility. C, D) Trends in research using the FST and TST. Data from Web of Science over the past two decades shows a steady increase in the number of publications involving the FST (C) and TST (D), highlighting their growing use in behavioral research. E-H) Test duration and analysis time in the FST and TST. We reviewed 50 recent studies using the FST (E, F) and 50 studies using the TST (G, H), recording both the total test duration and the time used for analysis. Most studies focused on the final 4-5 minutes of the test, rather than using the entire duration for analysis. I) Joint application of FST and TST. After excluding 16 duplicate studies, we assessed the concurrent use of both tests. The majority of studies employed both the FST and TST together in their experimental design. **J)** Averaged behavioral trajectory. The illustration shows a typical decline in swimming or struggling behavior over time, with intermittent fluctuations observed in the later stages of the test. Traditional analyses often focus on the final minutes of the test (green background), neglecting the earlier phases (grey background). The data in this panel is artificially generated for demonstration purposes. **K)** Conventional methods for behavioral analysis. Traditional approaches summarize total immobility times by presenting group mean, standard error of the mean (SEM), individual

data points, and statistical results. For demonstration, artificial data is used in this panel, with G1 and G2 representing two hypothetical experimental groups. **L)** Behavioral trajectories for individual mice. The cartoons highlight the complexity of behavior patterns, showing that even if a mouse remains immobile for half of the 6-minute test, distinct behavioral trajectories can emerge. Asterisks indicate significance differences between groups, as determined by the Mann–Whitney U test; ***$p < 0.001$.

2. Result

2.1. Tool for automatic behavior recognition

Current behavior metrics offer limited insights. To analyze the underlying cognitive processes, we need detailed behavioral trajectory data. Manual annotation of these trajectories is time-consuming and prone to subjective criteria, which compromises both accuracy and consistency. To address these challenges, we developed a tool for automatic annotation of animal behavior in the FST and TST. As shown in Figure 2A-D, the tool includes several key modules: frame calibration and region of interest (ROI) selection, passive motion elimination, active motion detection, and behavioral trajectory smoothing and binning.

The process begins with calibration and ROI selection. This module corrects for image distortion due to camera angles and allows users to define the region where mouse movement is expected, termed the ROI. Next, the passive motion elimination module filters out irrelevant movements, such as floating or swaying, which could otherwise result in false detections. This step enhances the accuracy of detecting active behaviors like swimming or struggling. The active motion detection module then identifies the mouse's state, whether it is swimming, struggling, or immobile, on a frame-by-frame basis. Finally, the behavioral trajectory smoothing and binning module smooths the data and bins it into 2-second intervals, producing a clean and reliable behavioral trajectory for further analysis and modeling.

We validated the tool's performance by comparing its results to human expert annotations. Significant correlations observed in both total immobility times (Figure 2E, left panels, FST: $r = 0.411$, $p = 0.002$; TST: $r = 0.823$, $p < 10^{-5}$, Pearson correlation) and in the ranking of immobility times (Figure 2E, right panels, FST: $r = 0.419$, $p = 0.001$; TST: $r = 0.720$, $p < 10^{-5}$, Spearman correlation). These findings demonstrate that the tool's outputs closely align with manual annotations, and all subsequent analyses will be based on data provided by this tool.

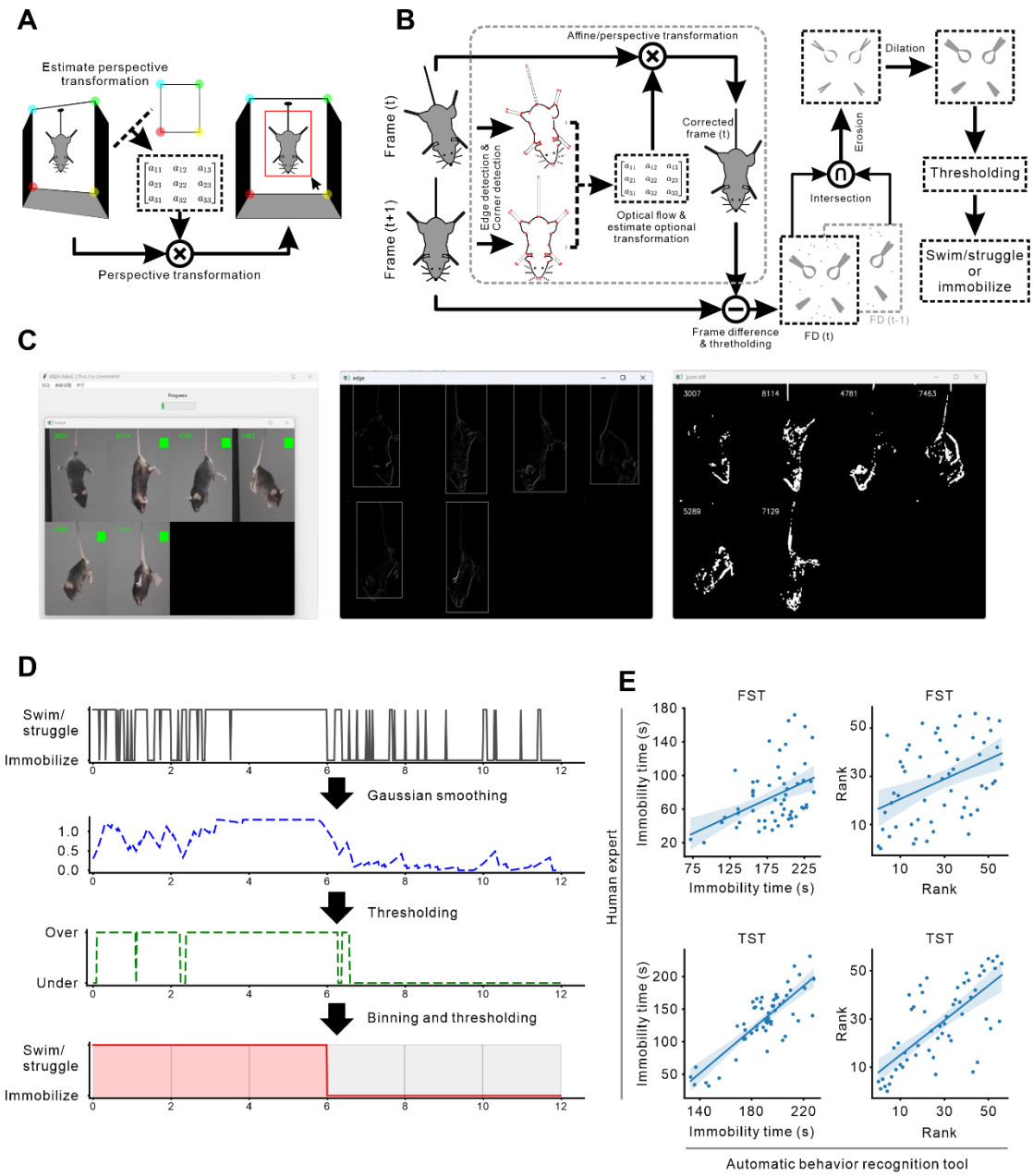

Figure 2. Tool for automatic annotation of animal behavior in the FST and TST. **A)** Frame calibration and ROI selection. To improve behavior recognition accuracy, raw video frames undergo perspective transformation based on camera angles. The user manually selects the four vertices of the experimental box in a chosen video frame, which are then compared to the pre-measured box dimensions. This process generates a perspective transformation matrix that corrects the frames. The region of interest (ROI) is then defined as the maximum area within which the mouse can move. **B)** Workflow of the custom-developed tool. The tool identifies behavioral states by calculating the differences between consecutive video frames. An optional module removes passive motion (e.g., floating or swinging) using geometric transformations to enhance accuracy. Noise reduction is achieved through morphological operations, followed by trajectory refinement using smoothing, binning, and thresholding techniques. **C)** Tool interface. The user-friendly interface enables efficient interaction with the tool, providing real-time

visualization of intermediate outputs from key processing steps. **D)** Smoothing and binning of behavioral trajectories. Raw behavioral trajectories are often noisy, as seen when a 6-second struggle is followed by 6 seconds of immobility, resulting in erratic data. Gaussian smoothing reduces this noise by assigns a behavioral value to each frame. Thresholding converts the smoothed trajectory into a binary profile, which is then binned into 2-second intervals to create a finalized, clear trajectory. E) Validation through expert comparison. The immobility times and their corresponding rankings generated by the tool exhibit strong correlations with expert evaluations, confirming the tool's reliability across both tests.

2.2. Behavior of mice in FST and TST

To induce depression-like behaviors, we employed two established experimental manipulations: chronic restraint stress (CRS) and chemogenetic inhibition of medial prefrontal cortex (mPFC) pyramidal neurons[50]. Comprehensive behavioral analyses were subsequently conducted to quantify immobility duration and behavior dynamics in the FST and TST under these conditions. In the CRS experiment, 29 C57BL/6 mice were housed under identical conditions and divided into two groups: a CRS group (n = 13), which underwent daily restraint stress for 6-8 hours over 21 days, and a control group (n = 16), which experienced no stress. On days 22 and 24, both groups underwent the FST and TST, respectively (Figure 3A). Behavioral trajectories and immobility times are shown in Figure 3B-G. The CRS group demonstrated significantly increased immobility time across both tests compared to the control group (FST: 202.15 ± 30.00 vs. 137.13 ± 77.02s, mean ± SD, $p = 0.024$; TST: 188.62 ± 59.89 vs. 130.50 ± 52.23, $p = 0.018$), and also showed higher immobility in the final 4 minutes of the FST (178.00 ± 20.96 vs. 118.75 ± 68.55, $p = 0.017$).

We next examined how chemogenetic inhibition of mPFC pyramidal neurons affects behavior in the FST and TST. A total of 24 C57BL/6 mice were randomly assigned to either a control group (n=12, AAV-CaMKIIα-mCherry) or an hM4D group (n=12, AAV-CaMKIIα-hM4D(Gi)-mCherry). Viral vectors were microinfused into the mPFC over 7 days (Figure 3H), followed by a 4-week expression period. Behavioral assessments using the FST and TST were conducted on days 36 and 38, respectively, with clozapine-N-oxide (CNO) administration preceding each test to activate the inhibitory hM4D receptors. Inhibition of mPFC neurons in the hM4D group increased immobility duration in the FST compared to controls, particularly after excluding an outlier mouse exhibiting persistent swimming behavior (Figure 3I-L, throughout: 216.73 ± 40.05 vs. 161.00 ± 60.36, $p = 0.060$; final 4 minutes: 176.73 ± 35.59 vs. 127.33 ± 59.25, $p = 0.049$).

These findings are consistent with existing literature but offer a more detailed analysis using our custom-developed tool. The tool allowed us to track behavioral trajectories, providing a richer dataset for more nuanced analysis. Notably, the probability of swimming and struggling typically decreases after the start of the test but shows a rebound and increased variability during the later stages. These dynamic behavioral patterns may reflect underlying cognitive processes in mice, laying a foundation for further exploration of cognitive mechanisms in depression-like behavior. Building upon this dataset, we propose to employ computational modeling approaches to elucidate the cognitive processes governing depression-like behavior.

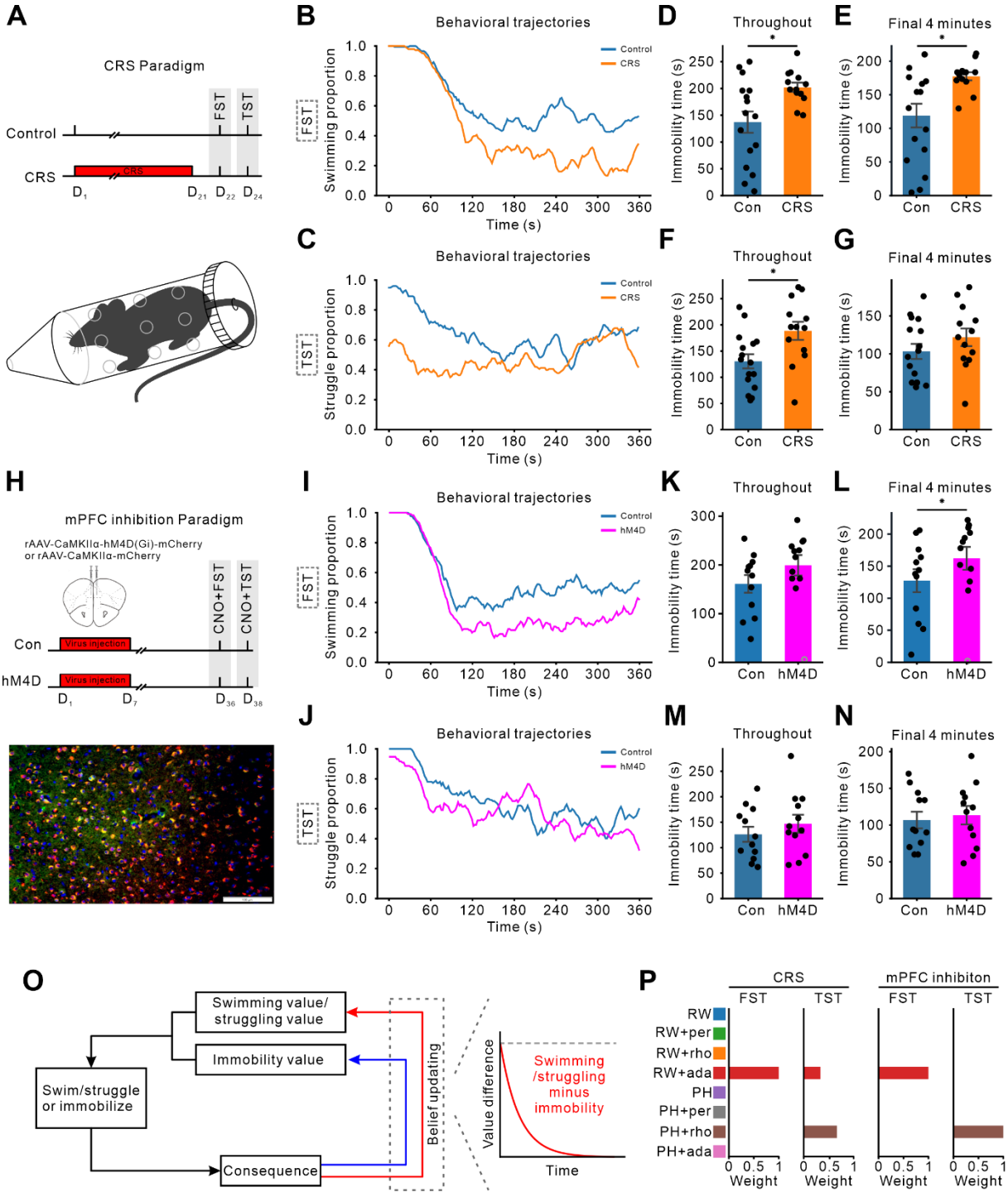

Figure 3. Behavior analysis of mice in FST and TST under two experimental manipulations**. A)** The chronic restraint stress (CRS) protocol. Following a 7-day acclimation period, 29 mice were randomly assigned to either a CRS group (n=13) or a control group (n=16). The CRS group underwent daily restraint stress from days 1 to 21, while the control group remained unstressed. Behavioral testing were conducted on days 22 (FST) and 24 (TST) for both groups. **B, C)** Behavioral trajectories in the FST and TST (CRS Experiment). Averaged behavioral trajectories are shown, with the control group represented in blue and the CRS group in yellow. **D-G)** Immobility duration in the FST and TST (CRS experiment). Immobility times for the FST (D, E) and TST (F, G) are shown for the entire testing period (D, F) and the final 4 minutes (E, G). Blue bars indicate the control group, yellow bars indicate the CRS group, and black dots represent individual animal data. Error bars denote the standard error of the mean (SEM). **H)** Chemogenetic inhibition of mPFC pyramidal neuron. After a 7-day acclimation period, 24 mice were evenly divided into control and hM4D groups. From days 1 to 7, the hM4D group received bilateral injections of rAAV-CaMKIIα-hM4D(Gi)-mCherry into the mPFC, while control mice were injected with rAAV-CaMKIIα-mCherry. Viral expression was allowed to mature for 28 days before behavioral testing, which was conducted on day 36 (FST) and day 38 (TST). Ninety minutes before testing, both groups received clozapine-N-oxide (CNO) injections, selectively inhibited pyramidal neuron activity in the hM4D group. Immunofluorescence confirmed hM4D(Gi)-mCherry expression in mPFC pyramidal neurons (red=hM4D(Gi), green=CaMKIIα, blue=DAPI; scale bar = 100 μm). Viral expression colocalized with pyramidal neurons at a rate of 89.27% (n=3 mice). **I, J)** Behavioral trajectories in the FST and TST (mPFC inhibition experiment). Averaged behavioral trajectories are shown, with the control group in blue and the hM4D group in magenta. **K-N)** Immobility duration in the FST and TST (mPFC inhibition experiment). Immobility times for the FST (K, L) and TST (M, N) follow the same format as panels D-G. Blue bars indicate the control group, while magenta bars represent the hM4D group. The hollow gray circles in panels K and L denote the outlier mice, which swam for nearly the entire test. **O)** Reinforcement learning model schematic. Within the reinforcement learning framework, mice begin by assigning expected values to two potential actions: swimming vs. immobility (FST) or struggling vs. immobility (TST). The selection of actions is determined by the difference in these expected values, which are continuously updated based on environmental feedback. Initially, swimming and struggling are assigned higher values as escape strategies. However, repeated failures to escape result in a reduction of these values, leading to increased immobility over time. **P)** Model weights across tests and experimental conditions. This bar plot shows model weights for different conditions, with colors indicating distinct models and bar lengths represent their weights. The winning model, defined as the one with the highest weight, is RW+ada for the FSTs and PH+rho for the TSTs across both experimental manipulations. Asterisks denote significant differences from the control groups, as determined by the Mann–Whitney U test; $^{**}p < 0.01$, $^{*}p < 0.05$.

2.3. Computational models for analyzing behavior in FST and TST

Reinforcement learning models have proven valuable in understanding the cognitive processes underlying behaviors in psychological and cognitive neuroscience research with human subjects. These models also hold significant promise for analyzing mouse behavioral trajectories in both the FST and TST. In this context, we conceptualize the mice as agents making decisions at each time step, aiming to optimize outcomes, either by maximizing rewards or minimizing punishments, through interactions with the experimental environment.

We hypothesize that, at each moment, mice decide between active coping behaviors, such as swimming or struggling, and passive coping behaviors, like immobility, based on their expectations of future consequences. These decisions will be continually re-evaluated and adjusted according to the consequences of previous actions, and may lead to shifts in behavioral preferences. For instance, early in the experiment, mice may perceive swimming or struggling as more valuable, believing that these actions could help them escape. However, the perceived value of these active behaviors declines with repeated failures, making immobility a more likely choice. This dynamic process of action re-evaluation, driven by updates from past experiences, is illustrated in Figure 3O.

To model this process, we fitted eight reinforcement learning models (described in detail in the Methods section), including the Rescorla-Wagner (RW) model and the Pearce-Hall (PH) model, along with their variants that incorporate sensitivity to consequences, behavioral perseveration, and consequences sensitivity adaptation. Bayesian model selection was used to identify the model that best captures the underlying cognitive processes. Models were compared using Bayesian bootstrap and model averaging, with weights assigned based on log-likelihood and model complexity. The weight of model indicates how likely the observed data is generated by this model. The model with the highest weight was selected as the “winning model”.

Figure 3P illustrates the winning models for both the FST and TST. An intriguing finding was that the winning models differed between the two tests. The RW+ada model emerged as the best fit for the FST, while the PH+rho model was most effective for the TST across both experimental manipulations. The RW+ada model updates beliefs with a fixed learning rate, while dynamically adjusting sensitivity to the consequences of actions. In contrast, the PH+rho model modulates the learning rate based on attention allocation, which is influenced by discrepancies between perceived and expected consequences, while maintaining fixed sensitivity to consequences. Importantly, both models successfully recovered their parameters (parameters in the RW+ada model: $r>0.52$, $p<0.001$; in the PH+rho model: $r>0.64$, $p<10^{-4}$; Pearson correlation), confirming their validity and reliability in capturing the obehavioral data.

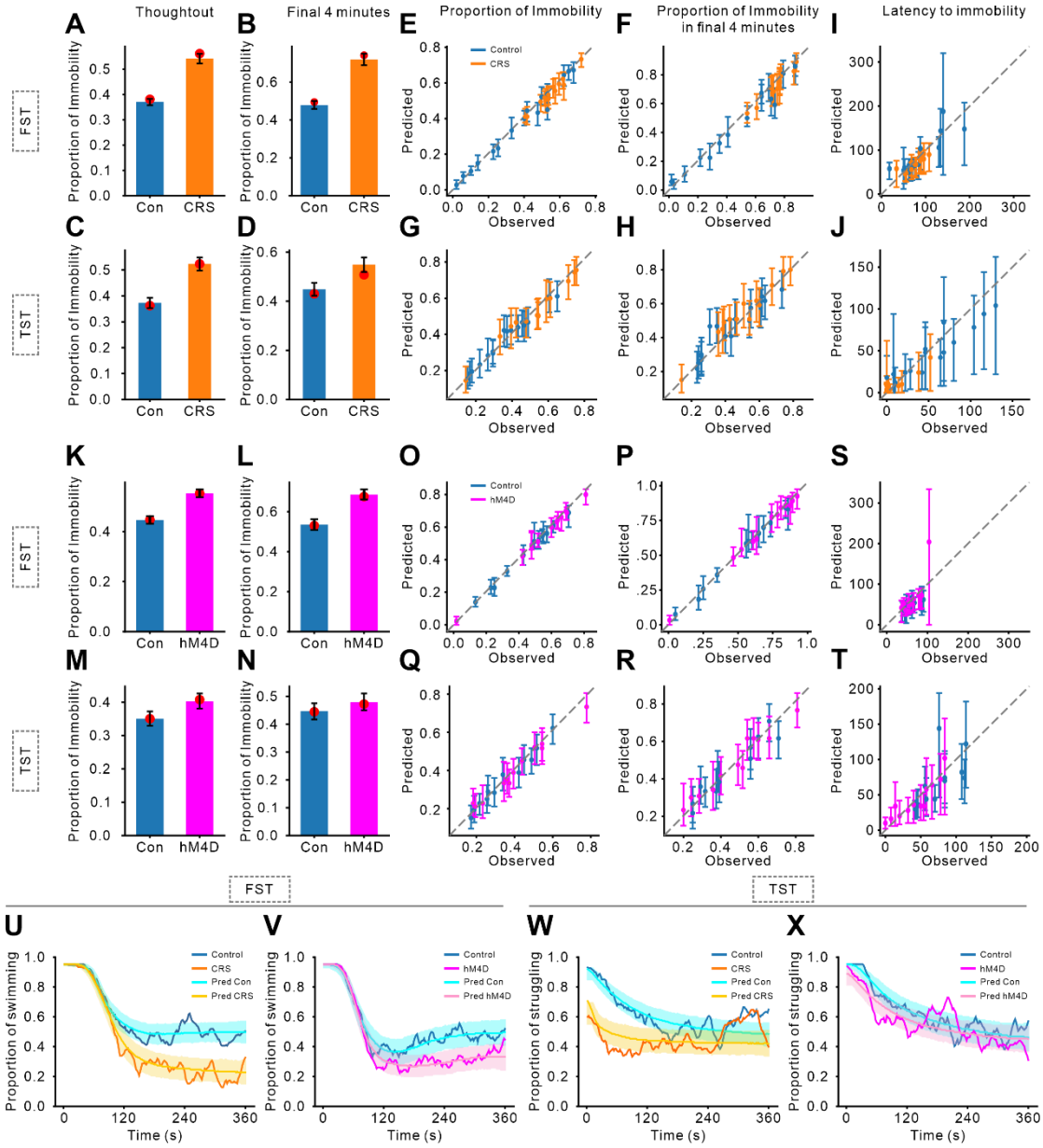

Figure 4. Posterior predictive checks for the winning models. A-D) Model-predicted vs. observed immobility proportions (CRS experiment, immobility vs. swimming/struggling). Panels A and B display the predicted immobility proportions for the FST, while panels C and D show the predictions for the TST. These predictions are compared with the observed proportions across the full testing period (A, C) and the final 4 minutes (B, D). The colored bars represent median predictions from the winning models, with error bars indicating the 95% highest density interval (HDI). Red dots mark the observed experimental averages, showing a strong alignment between the model predictions and actual data. **E-H)** Individual-level predicted vs. observed immobility proportions (CRS experiment). Panels E and F present comparisons of predicted and observed immobility proportions for individual mice in the FST, while panels G and H do the same for the TST. The x-axis represents observed values, and the y-axis shows median model predictions based on 2,000 simulations. Error bars denote the 95% HDI, with colors differentiating experimental

groups. **I, J)** Predicted vs. observed latencies to immobility (CRS experiment). Panels I and J show comparisons between the predicted and observed latencies to immobility in the FST and TST, formatted identically to panels E-H. K-N) Predicted vs. observed immobility proportions (mPFC inhibition experiment). Panels K-N replicate the analysis from panels A-D, but for the mPFC inhibition experiment, comparing predicted and observed immobility proportions. O-T) Individual-level predicted vs. observed immobility proportions and latencies (mPFC inhibition experiment). Panels O-T replicate the analysis from panels E-J, comparing individual-level predicted and observed immobility proportions and latencies in the mPFC inhibition experiment. **U-X**) Behavioral trajectories predictions. Panels U and V show predicted swimming behavior for the FST, while panels W and X display predicted struggling behavior for the TST across experimental groups. Cyan, yellow, and pink curves represent median predictions, with shaded areas indicating the 95% HDI based on 2000 simulations. Observed group averages are shown as blue, orange, and magenta lines. The models effectively capture behavioral dynamics, as most observed values fall within the 95% HDI.

2.4. Model validations

To assess the efficacy of these computational models, we conducted posterior predictive checks to evaluate how accurately the models predicted mouse behavior. As shown in Figure 4A-D and K-N, the winning models successfully captured the observed immobility proportions across all groups throughout the task and during the final 4 minutes. Additionally, nearly all individual immobility times fell within the simulated 95% highest density interval (HDI) (Figure 4E-H, and O-R), with strong correlations between the predicted and observed immobility times across all experimental conditions and time windows ($r>0.95$, $p<10^{-5}$, Pearson correlation). Figure 4I, J and S, T further show that the models made relatively accurate predictions of each mouse's latency to immobility ($r>0.71$, $p<0.001$, Pearson correlation). Moreover, the winning models successfully replicated the behavioral trajectories of the mice (Figure 4U-X), capturing the dynamic patterns of behavior over time. Collectively, these results confirm that the computational models provide a robust simulation of mouse behavior.

The model's success in simulating behavior indicate that the evolution of mouse behavior in both the FST and TST can be effectively described by reinforcement learning models, representing an ongoing process of learning, consequence perceiving, and decision-making. Furthermore, the differences between the winning models for these two tasks suggest that the cognitive processes driving behavior in the FST and TST are different. This challenges the common assumption that these two tests are interchangeable for cross-validation purposes, highlighting the need to consider different cognitive mechanisms underlying the behaviors observed in each task.

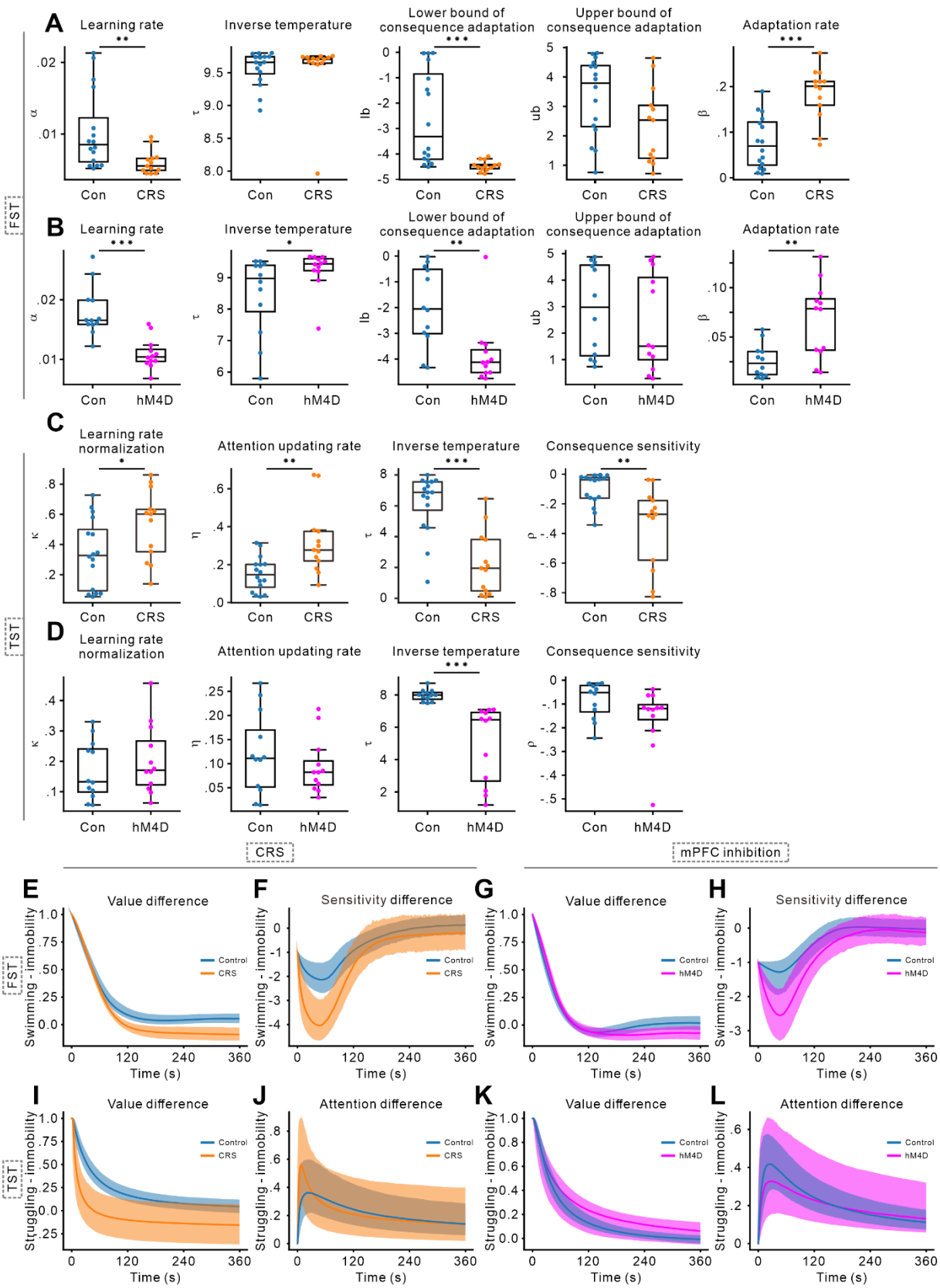

Figure 5. Comparison of model parameters. **A, B)** Parameter distributions for the winning model (RW+ada) in the FST. The RW+ada model for the FST includes five parameters: the learning rate (α), the inverse temperature parameter (τ), which reflects how strongly decision-making is influenced by differences in expected values, and two bound parameters for the adaptation of

consequence sesitivity—lb, which accounts for the intensification of negative experience following repeated escape failures during swimming, and ub, which captures the reduction of negative perception after prolonged immobility, the adaptation rate (β) governs the speed of these adjustments. Each panel displays one parameter, with individual data point representing the mean of 2,000 samples from each mouse. Boxplots illustrate the group-level medians and interquartile ranges, with blue, orange, and magenta representing the control, CRS, and hM4D groups, respectively. **C, D)** Parameter distributions for the winning model (PH+rho) in the TST. These panels following the same format as A and B, presenting the parameter distributions for the PH+rho model in the TST, which consists of four parameters: κ, which normalizes the learning rate; η, which determines the rate of attention updates; τ, which serves the same function as in the RW+ada model; and ρ, which quantifies the intensity of negative experiences following an escape failure. **E-H)** Predicted dynamics of expected value and consequence sensitivity in the FST. Panels E and F show the predicted differences in expected value (E) and adapted sensitivity to consequences (F) between swimming and immobility throughout the FST in the CRS experiment. Panels G and H display the same predictions for the mPFC inhibition experiment. Solid lines represent group-level medians, while shaded areas indicate the 95% HDI based on 2,000 posterior samples. **I-L)** Predicted dynamics of expected value and attention allocation in the TST. Panels I and J present the predicted differences in expected value (I) and attention allocation (J) between struggling and immobility in the CRS experiment, while panels K and L show the same predictions for the mPFC inhibition experiment. As in the FST panels, solid lines indicate group-level medians, with shaded areas representing the 95% HDI. Asterisks indicate significant differences compared to the control groups, as determined by the Mann–Whitney U test; ***$p < 0.001$, **$p < 0.01$, *$p < 0.05$.

2.5. Impact of CRS and mPFC inhibition on model parameters

The model parameters for each experimental group are presented in Figure 5A-D. In the FST, both the CRS and hM4D groups demonstrated significant reductions in the learning rate (α) and the lower bound of adaptation (lb) when compared to the control group. Additionally, the consequence sensitivity adaptation rate (β) was significantly increased in these groups. The hM4D group also showed a higher inverse temperature (τ). In the TST, both the CRS and hM4D groups had lower τ values than the control group. Furthermore, the CRS group exhibited higher learning rate normalization (κ) and attention updating rate (η), along with reduced sensitivity to consequences (ρ).

We further examined intermediate variables such as the expected value, adapted consequence sensitivity, and attention allocation over the course of the tests (Figure 5E-L). In general, the differences in expected value between swimming/struggling and immobility

decreased over time, reaching a stable, lower level. In the FST, both the CRS and hM4D groups showed lower value differences at later stages compared to the control group. In the TST, the CRS group exhibited a more rapid decline in expected value differences in the early stages, while there were no significant differences between the hM4D and control groups throughout the test. For relative consequence sensitivity, both the CRS and hM4D groups showed lower values in the early stages of the FST. In terms of attention allocation, the CRS group allocated slightly more attention to struggling behavior early in the TST compared to the control group.

The decrease in lb suggests that CRS and mPFC inhibition in the FST may lead to heightened feelings of despair in the mice after failed escape attempts. The increase in β likely accelerated this sense of despair, as illustrated by the yellow and magenta curves in Figure 5F and H, which consistently fall below the control group's (blue) curve, showing a steeper decline in the early stages. This shift resulted in a lower expected value for swimming (Figure 5E and G), ultimately contributing to a higher incidence of immobility. In the TST, the CRS group's early increase in η suggests that these mice more quickly attended to the discrepancy between expected and actual outcomes of struggling (Figure 5J, where the yellow line is above the blue line in the early stages). Coupled with a higher κ, this led to quicker learning of the negative consequences associated with struggling (Figure 5I, where the yellow line declines more rapidly), ultimately resulting in a faster onset of immobility.

2.6. Contribution of model parameters to behavior

To examine the influence of model parameters on behavior, we conducted simulations by varying two parameters at a time while holding others constant at their median values, which were derived from the posterior distribution of the winning models. The result of the FST and TST were shown in Figure 6 A-D and E-H, respectively. In the FST, we found that higher values of both the lower bound (lb) and upper bound (ub) of consequence sensitivity adaptation were associated with longer swimming durations. The relationship between α and β was more complex: very low α values prolonged swimming, while moderate β values, when combined with higher α, promoted swimming behavior. In the TST, longer struggling durations were linked to higher values of ρ, along with lower values of κ, η and τ.

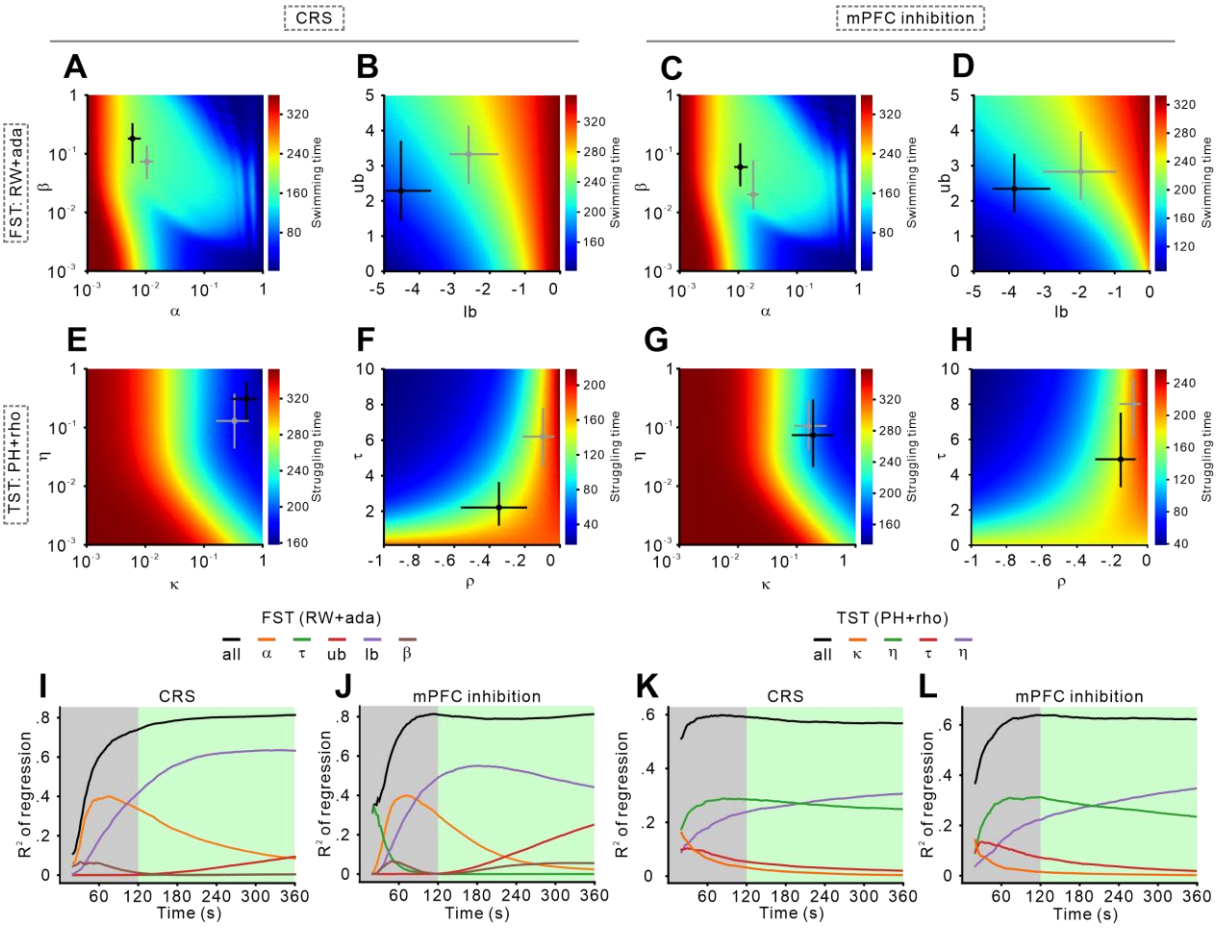

Figure 6. Linking model parameters to behavioral patterns. A-D) Simulated swimming durations by the RW+ada model. Heatmaps depict simulated total swimming times across the parameter space of the RW+ada models. Each heatmap explores the effects of two selected parameters while holding others fixed at their posterior median values. The x- and y-axes represent the sampled parameter values, with brighter colors indicating longer swimming durations. Circles mark the posterior median estimates, while horizontal and vertical lines indicate the 95% HDI. Black markers represent the CRS or hM4D groups, and gray markers indicate the control group. Panels A and B show results for the CRS experiment, while panels C and D correspond to the mPFC inhibition experiment. E-H) Simulated struggling durations by the PH+rho model. Similar to panels A-D, these heatmaps illustrate simulated struggling behavior by the PH+rho model. Panels E and F display results for the CRS experiment, while panels G and H correspond to the mPFC inhibition experiment. I-L) Explanatory power of model parameters for behaviors. Panels I-L present the explanatory power (r^2) of individual and combined model parameters from linear regression analyses predicting cumulative swimming (I, J) and struggling (K, L) times in the FST and TST. Black curves represent r^2 values for models incorporating all parameters, while colored curves show the explanatory power of individual parameters. Panels I and J correspond to the CRS experiment, while panels K and L display results for the mPFC inhibition experiment. Parameter contributions evolved over time: learning rate-related parameters (α, η) were most

influential in the early phases, whereas parameters tied to consequence sensitivity (lb, ub, ρ) gained importance in later stages.

To further explore the impact of model parameters on behavior in greater detail, we analyzed their relationship with behavioral performance at each time step. Linear regression models were used to predict cumulative swimming or struggling times based on parameters sampled from the posterior distribution of the winning models. The contribution of each parameter was assessed by comparing their explanatory power (r^2). This analysis revealed that different parameters exerted varying degrees of influence at different stages of the experiment. In the early stages of the FST, α from the RW+ada model was the strongest predictor of cumulative swimming time. However, as the experiment progressed, the influence of α diminished, while the bounds of consequence sensitivity adaptation (lb and ub) became more significant (Figure 6I, J). In the TST, η from the PH+rho model was the dominant factor early in the test, while ρ gained importance in the later stages (Figure 6K, L).

These findings suggest that traditional analytical methods, which often overlook early-phase data, may underestimate the role of learning rate-related factors and overemphasize consequence sensitivity when interpreting animal behavior.

3. Discussion

In this study, we introduced a custom-developed tool for analyzing animal behavior, enabling the efficient collection of detailed behavioral trajectories in the FST and TST. Our computational modeling analysis revealed that both behaviors in these tasks are driven by reinforcement learning processes involving learning, consequence perceiving, and decision-making. However, the underlying cognitive processes in the FST and TST differ, challenging the common assumption that these tasks are equivalent or mutually validating. By analyzing model parameters that represent different cognitive components, we found that CRS and mPFC inhibition primarily increased immobility in both tests by altering the learning rates and sensitivity of consequence. Additionally, our analysis showed that different cognitive components had varying impacts at different stages of the experiment. This suggests that traditional methods, which often exclude early-phase data, may underestimate the influence of learning-related factors while overemphasizing sensitivity to consequence. Overall, our findings emphasize that behavioral trajectories are a rich source of information, which, when carefully investigated through computational modeling, can reveal the complex cognitive processes driving behavior.

3.1. The necessity of using fine-grained behavioral trajectories

The FST and TST are commonly used to study depression-like behavior in rodents. As research into depression deepens, there is increasing interest in the cognitive insights these tests can offer. However, traditional metrics, which typically focus on immobility time in the final minutes as a single measure, fail to capture the complexity and evolution of behavior throughout the test. This limitation has hindered a comprehensive understanding of the cognitive processes involved in the FST and TST, highlighting the need for fine-grained behavioral trajectory data.

Currently, the identification of behaviors in the FST and TST relies heavily on labor-intensive manual annotation, often requiring second-by-second or frame-by-frame analysis. This process is not only time-consuming but also limits the broader adoption of behavioral trajectory analysis in research. To address these challenges, we developed a Python-based user-friendly tool for automatically tracking behavioral trajectories in the FST and TST. This tool provides frame-level temporal resolution, allowing researchers to identify animal action states with high precision. By using this tool to capture detailed behavioral trajectories, researchers can detect subtle changes in behavior, apply computational models, and gain deeper insights into the cognitive processes underlying animal behavior.

3.2. Using computational models to analyze behaviors in FST and TST

This study represents a pioneering effort to analyze mouse behavior in the FST and TST using reinforcement learning models, offering new insights into the cognitive processes at play. We framed the continuous decision-makings between swimming/struggling and immobility as reinforcement learning processes, and applying the classic Rescorla-Wagner (RW) and Pearce-Hall (PH) models, along with their variants, to model behavior.

While both RW and PH models predict that the expected values of actions gradually converge with perceived consequences over time, our observations of behavioral trajectories in the FST revealed a more dynamic pattern. Rather than stabilizing in the later stages, mouse behavior exhibited rebounds and fluctuations, with swimming behaviors resurfacing after extended periods of immobility. To better capture this complexity, we incorporated the adaptation of consequence sensitivity into our models. Consequence adaptation consists of two components—positive adaptation, which alleviates the negative subjective experiences associated with failed escape attempts after prolonged immobility, and negative adaptation, which amplifies the negative experiences resulting from repeated failures in swimming or struggling. Model that incorporated this adaptive factor emerged as the winning models for the

FST, accurately predicting immobility durations and capturing the dynamic evolution of behavior. This highlights the effectiveness of integrating adaptive processes into computational models for simulating behavior in this task.

3.3. Behavior in the FST and TST can be interpreted as reinforcement learning processes

Despite their widespread use, the cognitive processes assessed by the FST and TST remain insufficiently understood. Although the adaptive learning hypothesis is promising, it has not been rigorously supported with quantitative evidence. In this study, reinforcement learning models effectively captured the evolution of mouse behavior, predicting behavioral metrics both at the individual and group levels, as well as the behavioral trajectories in the FST and TST. These findings suggest that behavior in these tasks can indeed be interpreted as reinforcement learning processes, involving learning, consequence perceiving, and decision-making.

Specifically, when initially placed in an uncomfortable environment, mice evaluate swimming and struggling as potential escape strategies, assigning higher expected value to these actions. As a result, these actions are more frequently chosen in the early stages of the test. However, repeated failed escape leads to prediction errors—discrepancies between the expected value of these actions and the actual consequences. These prediction errors drive a continuous reassessment of the expected values of each behavior. Over time, the expected value of swimming and struggling diminishes, potentially falling below that of immobility, which results in the increased immobility observed in the later phases of the experiment.

3.4. FST and TST exam different cognitive processes

Although these tests share similar methodologies, our findings indicate that they engage different cognitive processes. The models that best fit the behavioral data for each task differ, suggesting that mice rely on different cognitive mechanisms in each task. In the FST, the RW+ada model provides the most accurate representation of behavior, implying that mice dynamically adjust their subjective experiences based on previous actions and consequences, updating their expected value at a fixed rate. Conversely, in the TST, the PH+rho model best captures the observed behavior, suggesting that mice alter their rate of learning based on attention allocation, which is influenced by discrepancies between expected and perceived consequences, while maintaining a stable perception of those consequences.

These results challenge the common practice of using the FST and TST interchangeably for cross-validation, as they underscore the differences in the cognitive processes driving behavior in each task. The FST appears to emphasize how animals dynamically perceive and adapt to the consequences of their actions, while the TST may be more focused on how attention modulates learning processes. This distinction may help explain the inconsistent results often observed when using these tests to evaluate depression-like behavior. Our findings point to the need for a more nuanced understanding of the cognitive processes measured by these behavioral assays, and we hope that future research will further elucidate these processes and develop more appropriate methods for cross-validation.

3.5. Limitation of traditional methods: overlooking learning and overemphasizing consequence sensitivity

Traditional metrics in the FST and TST often focus primarily on the final minutes of the tests, a practice that can lead to incomplete or potentially misleading conclusions. Our findings suggest that this approach may fail to capture the full complexity of behavior. Using computational models, we observed that, in the FST, the learning rate was the most influential factor in shaping behavior during the early stages. However, as the experiment progressed, its influence diminished, and the bounds of consequence sensitivity adaptation became more prominent. A similar pattern was observed in the TST. In the early phases, the rate of attention updating had the greatest influence, but as time went on, the role of consequence sensitivity became more dominant.

These shifts highlight the critical role of learning in the early stages of the tests, with consequence sensitivity taking a more prominent role in later phases. By disregarding the first two minutes of the experiment, a common practice, traditional methods risks underestimating the importance of learning, while overemphasizing the roles of consequence sensitivity. This oversight may limit our understanding of depressive-like behaviors and hinder the development of effective antidepressant treatments. To address this issue, we recommend that future studies focus on analyzing the full behavioral trajectory, utilizing computational models to gain a more comprehensive understanding of the cognitive processes driving behavior.

4. Methods

Subjects

Male C57Bl/6 mice (weighing 20–30g, 8 weeks old at the start of experiments) were obtained from Beijing SPF Animal Technology Co. for all experiments. The mice were housed under controlled conditions: a 12:12-hour light-dark cycle (lights on at 7:00 AM), a temperature of 25 ± 2°C, and humidity levels of 50 ± 10%. Behavioral experiments commenced after one week of acclimatization and were conducted.

Chronic restraint stress (CRS) model

The CRS procedure followed a widely accepted paradigm with slight modifications. In brief, mice were restrained in tubes with limited movement for 8 hours daily (10:00 AM–6:00 PM) over 21 consecutive days. Control mice were kept in their home cages without exposure to stress. After each restraint session, the mice were released and returned to their home cages. All experimental procedures were approved by the Institutional Animal Care and Use Committee (IACUC) of the Beijing Institute of Basic Medical Sciences (Approval number: IACUC-06-2019-002).

Stereotaxic surgeries and chemical genetics

Stereotaxic surgeries were performed under general anesthesia with 1% sodium pentobarbital using a stereotaxic apparatus (RWD Life Science Co., Ltd, Shenzhen, China). To inhibit pyramidal neurons in the mPFC, 500nL of rAAV-CaMKIIα-hM4D(Gi)-mCherry (BrainVTA Co., Ltd, Wuhan, China) was bilaterally injected into the mPFC (250nL for each side) of C57Bl/6 mice at the coordinates: AP +2.34 mm, ML ±0.3 mm, and DV −1.8 mm from Bregma. The control group received the same injection protocol but with rAAV-CaMKIIα-mCherry (BrainVTA Co., Ltd, Wuhan, China). The infusion was performed using a glass pipette connected to a Hamilton syringe fitted with a 33-gauge needle. The syringe was mounted on a syringe pump (RWD Life Science Co.) to ensure precise control over the infusion process. The infusion rate was set to 50 nl/min, allowing for consistent and accurate delivery of the solution. The injection pipette was slowly withdrawn 10 minutes after the infusion. Behavioral experiments were conducted 4 weeks post-surgery.

On the day of the testing, Clozapine N-oxide (CNO) was administered intraperitoneally to inhibit pyramidal neurons(5mg/kg), and behavioral assessments began 90 minutes later. After the behavioral tests, the mice were perfused, and whole brains were collected for immunofluorescent staining to verify viral transduction. The results confirmed successful infection of 89.27% of pyramidal neurons, ensuring effective viral expression.

Forced swim test (FST) and tail suspension test (TST)

The FST was conducted in a well-lit room where mice were individually placed in water-filled cylinders (35 cm height × 10 cm diameter) with water maintained at 24–25°C. The water depth was sufficient to prevent the mice from touching the bottom with their limbs. Mice were allowed to swim freely for about 6 minutes while their movements were recorded on video.
For the TST, mice were gently removed from their cages, and their tails were secured with adhesive tape approximately 1 cm from the tip. The mice were then suspended by their tails, with the distance between the tip of the tail and the ground set at approximately 30 cm, placing the mice in an inverted position. The test lasted for approximately 6 minutes, and video recordings of the mice's behavior were obtained during the experiment.

Tool for automated behavioral recognition

In brief, the automated behavior recognition tool consists of four modules: the Calibration and Region of Interest (ROI) Selection module, the Passive Motion Compensation module, the Active Motion Detection module, and the Smooth and Thresholding Analysis module. We briefly describe the function of each module below.

1. *Calibration and ROI Selection Module:* As shown in Figure 2A, we mitigate the impact of camera angles on recognition accuracy by applying a perspective transformation to the original images. Prior to detection, the user manually selects the coordinates of the experimental box's vertices in the video frame. By comparing these coordinates with pre-measured box dimensions, we calculate and apply a perspective transformation matrix to correct the original video frames. On the corrected frames, the largest possible movement area of the mouse is defined as the ROI. The tool offers two options for selecting the ROI: manually adjusting the size by dragging the mouse or choosing from preset sizes. The selected ROI is resized to 360×480 pixels for further analysis.

2. *Passive Motion Compensation Module (Optional):* As illustrated in the dashed box in Figure 2B, this module focuses on analyzing the animal's contour map extracted from the region of interest (ROI), along with key points required for estimating optical flow. Optical flow techniques are used to track these key points in successive frames. In cases where the animal is passively moving, such as during inertial drift or pendulum motion, its posture remains static. Consequently, the relative positions of key points between adjacent frames remain constant, indicating only an overall shift. The Pyramid Lucas-Kanade optical flow algorithm is applied to detect corresponding key points in the following frame. By minimizing the geometric distance between predicted and actual key point positions, the algorithm determines the

geometric transformation that best represents the animal's overall movement. This fitted transformation models the passive motion of the animal. Using this module, the current frame is adjusted to generate a passive motion-compensated prediction, enabling direct comparison with the subsequent frame for further analysis.

3. Active Motion Detection Module: As shown in Figure 2B, active movement by the animal results in significant differences between adjacent frames, even after passive motion compensation. We use a three-frame differencing method to calculate inter-frame differences based on the ROI images from frames t and t+1. These differences are then applied a threshold to generate a binary difference image at frame t, which is combined with a cached binary difference image from frame t-1 using intersection operations. Morphological operations (erosion and dilation) are adopted to remove noise, and the processed image is then summed and thresholded to determine the movement state (struggling or immobilize). Figure 2C displays the current video frame, contour detection results (if passive motion compensation is enabled), and combined inter-frame differences to illustrate the tool's effectiveness.

4. Behavioral Trajectory Smoothing and Binning Module: As illustrated in Figure 2D, the original behavioral trajectory for each frame often contains significant noise. For example, in a video where a mouse struggles for the first 6 seconds and remains immobile for the following 6 seconds, initial recognition may produce noisy results, as shown in the top row. To address this, Gaussian smoothing is applied to reduce noise and produce a clearer trajectory, as depicted in the second row. Next, thresholding is used to convert the smoothed data into a binary trajectory, shown in the second row from the bottom. Finally, the data is processed through binning and an additional thresholding step, resulting in a behavior trajectory with 2-second bins. This final trajectory, shown in the bottom row, is both more accurate and robust for subsequent analysis.

Reinforcement learning models

We employed reinforcement learning models to fit the behavioral trajectories observed in the FST and TST. In this framework, mice are treated as agents with the goal of optimizing outcomes, which includes maximizing rewards and minimizing punishments. Specifically, the mice make decisions based on their value expectations about actions, and update the value expectations by calculating prediction errors between value expectations and actual outcomes. Future action decisions are made based on these updated values. We implemented 8 reinforcement learning models to explore different value updating mechanisms and cognitive processes underlying behaviors in FST and TST.

1. Rescorla-Wagner model (RW): The Rescorla-Wagner model is a classic model of error-driven predictive learning. It assumes that mice update their beliefs by incorporating a fixed proportion of prediction error. Given that swimming and struggling deplete the mice's physical energy, making the subsequent failing to escape experiences more unpleasant than remaining immobile, we encoded the consequence of swimming and struggling as -1, while immobility was encoded as 0. The predictive error at timestep t was calculated as follows:

$$\delta_t = \begin{cases} -1 - Q_{a,t} & swim/strggle \\ 0 - Q_{a,t} & immobilize \end{cases}$$

The value expectation was updated as:

$$Q_{a,t+1} = Q_{a,t} + \alpha\delta_t$$

Here, δ_t represents the prediction error at timestep t, while $Q_{a,t}$ and $Q_{a,t-1}$ represent the value expectations for the actions taken by the mice at timesteps t and t-1, respectively. The parameter α is the learning rate, which governs the extent to which the prediction error is integrated into the updated value expectation.

A sigmoid function was applied to compute the probability of swimming/struggling based on the values expectation of actions. At each trial t, the probability of swimming/struggling $p_{s,t}$ was given by:

$$p_{s,t} = \frac{1}{1 + e^{-\tau(Q_{s,t} - Q_{i,t})}}$$

In this equation, $Q_{s,t}$ and $Q_{i,t}$ represent the value expectations of swimming/struggling and immobility, respectively. The probability of immobility is $1-p_{s,t}$. This decision function was adopted by RW, RW+rho, RW+ada, PH, PH+rho, and PH+ada models.

2. RW model with perseveration (RW+per): Building on the RW model, this model incorporates the influence of behavioral perseveration on the decision-making process. Behavioral perseveration is modeled based on the frequency of unchosen actions $uct_{a,t}$, which is updated according to the following rule:

$$uct_{a,t} = \begin{cases} 0 & if\ the\ action\ was\ not\ taken\ at\ t-1 \\ uct_{a,t-1} + 1 & if\ the\ action\ was\ taken\ at\ t-1 \end{cases}$$

The $uct_{a,t}$ are considered in decision. At each trial t, the probability of swimming/struggling $p_{s,t}$ was given by:

$$p_{s,t} = \frac{1}{1 + e^{-(\tau(Q_{s,t} - Q_{i,t}) + \phi(uct_{s,t} - uct_{i,t}))}}$$

Where $uct_{s,t}$ and $uct_{i,t}$ refers to the unchosen time for swimming/struggling and immobile, respectively. ϕ refers to the importance of perseveration.

3. RW model with consequence sensitivity (RW+rho): Building on the RW learning rule, this model incorporates the sensitivity to the consequence of swimming and struggling. The sensitivity to the consequence is represented by the parameter ρ. In this model, after swimming or struggling, the predictive error is computed as follows:

$$\delta_t = \rho - Q_{a,t}$$

This adjustment reflects the idea that the mice perceive the consequences of their actions (e.g., swimming and struggling) with varying degrees of sensitivity, as captured by ρ .

4. RW model with consequence sensitivity adaptation (RW+ada): This model further extends the RW learning rule by accounting for the adaptation of the mice's sensitivity to the consequence of actions. We hypothesize that repeated failed escape attempts through swimming or struggling or after prolonged reliance on immobility lead to changes in perceiving consequence of actions. The adaptation process is described as:

$$\rho_t^{ada} = \begin{cases} \beta(lb - \rho_{t-1}) & swim/strggle \\ \beta(ub - \rho_{t-1}) & immobilize \end{cases}$$

Here, the adapted consequence sensitivity ρ_t^{ada} replaces the fixed parameter ρ from the previous model, with β representing the rate of adaptation. The lower and upper bounds of sensitivity adaptation are represented by parameters lb and ub, respectively. The prediction error is then updated as:

$$\delta_t = \begin{cases} \rho_t^{ada} - Q_{a,t} & swim/strggle \\ 0 - Q_{a,t} & immobilize \end{cases}$$

5. Pearce-Hall (PH) Model: Unlike the Rescorla-Wagner rule, which assumes a constant learning rate, the Pearce-Hall model dynamically adjusts the learning rate based on the level of surprise or unpredictability. The value expectation is updated as follows:

$$Q_{a,t} = Q_{a,t-1} + \kappa a_{a,t}\delta$$

Here, $a_{a,t}$ represents the attention allocated to the action at time t, κ is a normalization parameter for learning rate. The attention $\alpha_{a,t}$ is updated based on the prediction error δ_t as follows:

$$a_{a,t+1} = (1 - \eta)a_{a,t} + \eta|\delta_t|$$

Where η refers to the updating rate for attention.

6. PH model with perseveration (PH+per): Combines the PH learning rule with perseveration, as defined in the RW+per model.

7. PH model with consequence sensitivity (PH+rho): Combines the PH learning rule with consequence sensitivity, as defined in the RW+rho model.

8. PH Model with consequence sensitivity adaptation (PH+ada): Combines the PH learning rule with consequence sensitivity adaptation, as defined in the RW+ada model.

Hierarchical Bayesian models

We used a hierarchical Bayesian framework to model individual behavioral trajectories. This approach allowed us to estimate participant-specific parameters while simultaneously leveraging data from the entire experimental group to improve estimation precision. Specifically, individual parameters were drawn from group-level distributions as follows:

$$param_{individual} = \mu_{group} + \sigma_{group} * var_{individual}$$

Here, $param_{individual}$represents the parameter for each individual mouse, μ_{group} and σ_{group} are the group-level mean and standard deviation of the parameter, respectively, and $var_{individual}$ refers to the individual-level variance. This hierarchical structure effectively captures both individual differences and shared underlying processes, offering a robust and nuanced representation of the observed behavioral dynamics.

Parameter estimation and model selection/validation

Parameter estimation was conducted using hierarchical Bayesian analysis (HBA) implemented in the Stan language[51] via Python (cmdstanpy[52]). Posterior inference was performed through Markov chain Monte Carlo (MCMC) sampling. The models were fitted separately for each and each test. The Gelman-Rubin convergence diagnostic (R-hat) was applied to assess MCMC stability. With all R-hat statistics falling within the recommended threshold of 1.05, the chains exhibited sufficient mixing and stationarity, supporting the reliability of posterior estimates.

Model comparison was used to evaluate how well the models fit the data, accounting for model complexity. Model comparison was assessed using Bayesian bootstrap and model averaging, wherein the log-likelihoods of each model were evaluated based on the posterior simulations, and a weight was assigned to each model. The model weights included a penalization term for complexity and a normalization term relative to the number of models being compared. For each group, the model weights summed to 1. The model with the highest weight was defined as the "winning model," indicating that it best fit the observed behavioral data of the mice.

To perform a posterior predictive check, we simulated behavioral trajectories for each animal in each experimental manipulations and test, based on the parameters of the winning model. Specifically, the model generated random draws from each animal's joint posterior

distribution to predict actions. This process was repeated 2,000 times per animal for each test. We compared each animal's synthetic data to their experimental observations, focusing on the immobility times both throughout the test and in the final 4 minutes, the first immobile time, and the behavioral trajectories of mice.

Histology and microscopy

Following the final day of the behavioral experiments (Figure 5), mice were injected with 0.2 mL of a urethane solution at a concentration of 0.3 mg/mL to achieve anesthesia. Subsequently, they underwent transcardial perfusion with 4% paraformaldehyde in PBS for fixation. The brains were then post-fixed overnight, and coronal brain sections (20 μm) were prepared. Cell samples were imaged using a fluorescent microscope, and images were analyzed using ImageJ Pro Plus Version 6.0 (Bethesda, Maryland, USA).

Analysis of trends in research publications

To examine the research trends involving the FST and TST, the annual number of publications from 1995 to 2024 was collected from the Web of Science database. The analysis followed a two-step query process to ensure specificity to studies related to affective and stress-related disorders as well as the FST and TST.

The initial query used the following terms to identify publications related to affective and stress-related disorders:

TS = ((depression) OR (depressed) OR (depressive) OR (dysthymia) OR ("affective disorder") OR ("mood disorder") OR (anhedonia) OR (despair) OR (helplessness) OR (anxiety) OR (stress) OR ("social defeat")).

This search was refined by adding terms specific to the FST or TST. For the FST, the query was:

TS = ((FST) OR ("Forced Swimming Test") OR ("Forced Swim Test")).

For the TST, the query was:

TS = ((TST) OR ("tail suspension test") OR ("suspension test") OR (tail-hanging test)).

The results from each refined search were categorized by year of publication to analyze annual trends. The data were visualized as a bar graph to illustrate the temporal progression of research activity in the field.

Statistics

Comparative statistical tests, correlation analyses, and linear regressions were conducted using Python libraries, including SciPy[53] and scikit-learn[54]. Mann-Whitney U tests were conducted to compare differences in immobility times between groups (Figs. 3B-G, I-N) and differences in model parameters across groups (Figure 5A-D). Pearson correlation analysis was used to examine the relationships between the posterior predictive mean of immobility time and the latency to immobility for each individual with their corresponding experimental observations (Figs. 4E-J, O-T). Additionally, Pearson correlation was applied to evaluate the agreement between immobility times identified by the automated recognition tool and those identified by human experts. Spearman correlation analysis was employed to assess the ranking consistency of immobility times identified by the automated tool and human experts. The linear regression models shown in Figs. 6G-J used model parameters as inputs to predict cumulative immobility times at each time step.

Acknowledgements

This work was supported by the National Natural Science Foundation of China (No. 32300853) and the STI2030-Major Projects (No. 2022ZD0208200 and No. 2021ZD0200900).

Author contributions

Z.L., and Y.L. conceived the project. Z.L., T.L., J.Y., and X.Z. performed the original experiments. Z.L. developed the tool for automated behavioral recognition and computational models, designed and performed analysis. Z.L., T.L., and Y.L. discussed the results and wrote the manuscript.

References

[1] G. J, B. Lg, G. M, *Nature reviews. Neuroscience* **2018**, *19*.
[2] C. M. Powell, T. Miyakawa, *Biological Psychiatry* **2006**, *59*, 1198.
[3] B. Ellenbroek, J. Youn, *Disease Models & Mechanisms* **2016**, *9*, 1079.
[4] M. Baker, S.-I. Hong, S. Kang, D.-S. Choi, *Laboratory Animal Research* **2020**, *36*, 9.
[5] A. A. Fenton, *Biological Psychiatry* **2015**, *77*, 1079.
[6] I. J. Makowska, D. M. Weary, *Applied Animal Behaviour Science* **2013**, *148*, 1.
[7] A. H. C. Wong, S. A. Josselyn, *Biological Psychiatry* **2016**, *79*, 32.
[8] Y. Shemesh, A. Chen, *Mol Psychiatry* **2023**, *28*, 993.
[9] M. L. Molendijk, E. R. de Kloet, *European Journal of Neuroscience* **2022**, *55*, 2813.
[10] L. Chen, G. C. Faas, I. Ferando, I. Mody, *Transl Psychiatry* **2015**, *5*, e551.
[11] S. Reardon, *Nature* **2019**, *571*, 456.
[12] A. Can, D. T. Dao, C. E. Terrillion, S. C. Piantadosi, S. Bhat, T. D. Gould, *J Vis Exp* **2012**, 3769.
[13] Y. Stukalin, A. Lan, H. Einat, *Neuroscience & Biobehavioral Reviews* **2020**, *112*, 39.
[14] J. M. De Pablo, A. Parra, S. Segovia, A. Guillamón, *Physiology & Behavior* **1989**, *46*, 229.

[15] M. L. Molendijk, E. R. De Kloet, *Psychoneuroendocrinology* **2015**, *62*, 389.
[16] E. R. de Kloet, M. L. Molendijk, *Neural Plasticity* **2016**, *2016*, 6503162.
[17] M. L. Molendijk, E. R. de Kloet, *Behavioural Brain Research* **2019**, *364*, 1.
[18] J. Anyan, S. Amir, *Neuropsychopharmacol.* **2018**, *43*, 931.
[19] A. Armario, *Neuroscience & Biobehavioral Reviews* **2021**, *128*, 74.
[20] L. Zhang, L. Lengersdorff, N. Mikus, J. Gläscher, C. Lamm, *Social Cognitive and Affective Neuroscience* **2020**, *15*, 695.
[21] W.-Y. Ahn, N. Haines, L. Zhang, *Computational Psychiatry* **2017**, *1*, 24.
[22] T. Kube, R. Schwarting, L. Rozenkrantz, J. A. Glombiewski, W. Rief, *Biological Psychiatry* **2020**, *87*, 388.
[23] I. M. Berwian, J. G. Wenzel, A. G. E. Collins, E. Seifritz, K. E. Stephan, H. Walter, Q. J. M. Huys, *JAMA Psychiatry* **2020**, *77*, 513.
[24] Q. J. M. Huys, N. D. Daw, P. Dayan, *Annual Review of Neuroscience* **2015**, *38*, 1.
[25] Q. J. Huys, D. A. Pizzagalli, R. Bogdan, P. Dayan, *Biology of Mood & Anxiety Disorders* **2013**, *3*, 12.
[26] D. Crawley, L. Zhang, E. J. H. Jones, J. Ahmad, B. Oakley, A. S. J. Cáceres, T. Charman, J. K. Buitelaar, D. G. M. Murphy, C. Chatham, H. den Ouden, E. Loth, the E.-A. L. Group, *PLOS Biology* **2020**, *18*, e3000908.
[27] V. M. Brown, L. Zhu, A. Solway, J. M. Wang, K. L. McCurry, B. King-Casas, P. H. Chiu, *JAMA Psychiatry* **2021**, *78*, 1113.
[28] A. Y. Dombrovski, K. Szanto, L. Clark, C. F. Reynolds, G. J. Siegle, *JAMA Psychiatry* **2013**, *70*, 1020.
[29] L. Zhang, J. Gläscher, *Science Advances* **2020**, *6*, eabb4159.
[30] J. Halim, A. H. Robinson, J. F. Navas, C. Martin-Perez, R. Vilar-Lopez, T. T.-J. Chong, A. Verdejo-Garcia, *Appetite* **2023**, *183*, 106484.
[31] P. Homan, I. Levy, E. Feltham, C. Gordon, J. Hu, J. Li, R. H. Pietrzak, S. Southwick, J. H. Krystal, I. Harpaz-Rotem, D. Schiller, *Nature Neuroscience* **2019**, *22*, 470.
[32] C. Langley, S. Armand, Q. Luo, G. Savulich, T. Segerberg, A. Søndergaard, E. B. Pedersen, N. Svart, O. Overgaard-Hansen, A. Johansen, C. Borgsted, R. N. Cardinal, T. W. Robbins, D. S. Stenbæk, G. M. Knudsen, B. J. Sahakian, *Neuropsychopharmacology 2023 48:4* **2023**, *48*, 664.
[33] C. Feher da Silva, T. A. Hare, *Nat Hum Behav* **2020**, *4*, 1053.
[34] C. Chen, T. Takahashi, S. Nakagawa, T. Inoue, I. Kusumi, *Neuroscience & Biobehavioral Reviews* **2015**, *55*, 247.
[35] Q. J. M. Huys, T. V. Maia, M. J. Frank, *Nature Neuroscience* **2016**, *19*, 404.
[36] D. C. L. Lan, M. Browning, *Computational Psychiatry* **2022**, *6*, 166.
[37] S. Palminteri, M. Lebreton, *Trends in Cognitive Sciences* **2022**, *26*, 607.
[38] T. Kube, L. Rozenkrantz, *Perspect Psychol Sci* **2021**, *16*, 247.
[39] T. Katthagen, S. Fromm, L. Wieland, F. Schlagenhauf, *Frontiers in Psychiatry* **2022**, *13*.
[40] V. B. Gradin, P. Kumar, G. Waiter, T. Ahearn, C. Stickle, M. Milders, I. Reid, J. Hall, J. D. Steele, *Brain* **2011**, *134*, 1751.
[41] P. Kumar, G. Waiter, T. Ahearn, M. Milders, I. Reid, J. D. Steele, *Brain* **2008**, *131*, 2084.
[42] P. Kumar, F. Goer, L. Murray, D. G. Dillon, M. L. Beltzer, A. L. Cohen, N. H. Brooks, D. A. Pizzagalli, *Neuropsychopharmacology 2018 43:7* **2018**, *43*, 1581.
[43] A. C. Pike, O. J. Robinson, *JAMA Psychiatry* **2022**, *79*, 313.
[44] H. Bottemanne, O. Morlaas, A. Claret, T. Sharot, P. Fossati, L. Schmidt, *JAMA Psychiatry* **2022**, *79*, 1124.
[45] C. Liao, A. C. Kwan, *Chronic Stress* **2021**, *5*.
[46] H. R. Kim, A. N. Malik, J. G. Mikhael, P. Bech, I. Tsutsui-Kimura, F. Sun, Y. Zhang, Y. Li, M. Watabe-Uchida, S. J. Gershman, N. Uchida, *Cell* **2020**, *183*, 1600.

[47] A. Dezfouli, R. Morris, F. Ramos, P. Dayan, B. W. Balleine, *Advances in Neural Information Processing Systems* **2018**, *2018-Decem*, 4228.
[48] W. Dabney, Z. Kurth-Nelson, N. Uchida, C. K. Starkweather, D. Hassabis, R. Munos, M. Botvinick, *Nature* **2020**, *577*, 671.
[49] J. P. H. Verharen, J. W. de Jong, Y. Zhu, S. Lammel, *Nat Commun* **2023**, *14*, 2419.
[50] V. S. Sohal, J. L. R. Rubenstein, *Molecular Psychiatry* **2019**, *24*, 1248.
[51] Documentation, .
[52] cmdstanpy – Python interface to CmdStan — CmdStanPy 1.2.4 documentation, .
[53] SciPy 1.0: fundamental algorithms for scientific computing in Python | Nature Methods, .
[54] F. Pedregosa, G. Varoquaux, A. Gramfort, V. Michel, B. Thirion, O. Grisel, M. Blondel, P. Prettenhofer, R. Weiss, V. Dubourg, J. Vanderplas, A. Passos, D. Cournapeau, M. Brucher, M. Perrot, É. Duchesnay, *J. Mach. Learn. Res.* **2011**, *12*, 2825.